PLANETARY SCIENCE

Submicroscopic magnetite may be ubiquitous in the lunar regolith of the high-Ti region

Zhi Cao[1,2]†, Zhuang Guo[1,3]†, Chen Li[1], Sizhe Zhao[1,4], Yang Li[1,5]*, Qi He[2]*, Yuanyun Wen[1], Zhiyong Xiao[6], Xiongyao Li[1,5], Long Xiao[2], Lifang Li[7], Junhu Wang[8], Jianzhong Liu[1,5]

Magnetite is rare on the Moon. The ubiquitous presence of magnetite in lunar soil has been hypothesized in previous Apollo Mössbauer spectroscopy and electron spin resonance studies, but there is currently no mineralogical evidence to prove it. Here, we report a large number of submicroscopic magnetite particles embedded within iron-sulfide on the surface of Chang'e-5 glass, with a close positive correlation between magnetite content and the TiO_2 content of the surrounding glass. The morphology and mineralogy of the iron-sulfide grains suggest that these magnetite particles formed via an impact process between iron-sulfide droplets and silicate glass melt, and ilmenite is necessary for magnetite formation. Magnetite in lunar glass is a potential candidate for the "magnetite-like" phase detected in the Apollo era and suggests that impact-induced submicroscopic magnetite may be ubiquitous in high-Ti regions of the Moon. Moreover, these impact-induced magnetite particles may be crucial for understanding the lunar magnetic anomalies and mineral components of the deep Moon.

INTRODUCTION

Magnetite is an important oxidized mineral in planetary science, involved in key questions related to paleomagnetic fields and indicators of life. It is commonly believed to be rare on the reduced lunar surface (*1*–*4*). Although Mössbauer spectroscopy and electron spin resonance (ESR) studies have hypothesized the prevalence of submicroscopic "magnetite-like" phases in Apollo lunar soils, there is no correlative mineralogical evidence for their genesis and potential distribution on the Moon (*1*, *5*–*10*).

Previous studies have proposed several mechanisms for the production of magnetite on the Moon, driven either by common lunar interior oxidation conditions (*9*, *11*, *12*) or by direct input of exogenous material (*13*–*15*), giving new insights into localized higher oxygen fugacity environments specific to the Moon. However, it is important to emphasize that the presence of individual magnetite particles produced by various formation mechanisms is incidental and independent, and it is hard to extend to the global lunar surface. The formation mechanism of magnetite on the lunar surface still needs to be fully discussed.

Impacts play a dominant role in the construction and reworking of lunar regolith, and they have markedly altered the chemical and structural characteristics of lunar surface materials and complicated their mineralogy (*16*). In particular, recent analysis has revealed the impact-induced formation of Fe^{3+} and magnetite in Chang'e-5 lunar soils, implying a possible ubiquitous presence of oxidized iron on the lunar surface under conditions of continuous meteorite bombardment (*17*, *18*). In addition, magnetite is difficult to recognize spectroscopically using remote sensing owing to its dark color and opacity (*3*, *4*). Therefore, its distribution can only be inferred from lunar samples by identifying suitable conditions for its formation mechanism.

Here, we systematically studied the microscopic characteristics of iron-sulfide droplets in Chang'e-5 lunar soil, and revealed that the genesis of magnetite inside iron-sulfide grains is related to the ilmenite-bearing glass in which they are embedded. The magnetite content within the iron-sulfide grains positively correlates with the content of surrounding Ti-rich material. We propose that magnetite in this form within iron-sulfide grains provides in situ mineralogical proof of the submicroscopic magnetite-like phases recognized during the Apollo era.

RESULTS

Iron-sulfide grains in Chang'e-5 glass

A large number of droplet-like, rounded iron-sulfide grains with unique surface microscopic features embedded within impact glasses of various compositions in Chang'e-5 lunar soil were identified using scanning electron microscopy (SEM) (Fig. 1, A to C, and fig. S1). The boundary between each iron-sulfide grain and the surrounding glass was coupled in shape with sharp compositional differences, consistent with the dented microstructure on Chang'e-5 glass surfaces described by Yan *et al.* (*19*); this likely implies an impact process (*20*–*24*). In addition, metallic iron of variable size (30 to 500 nm) sparsely protruded and covered the entire surface of each rounded iron-sulfide grain (Fig. 1, D to F). Iron-sulfide grains embedded within high-Ti (25.5 wt %), medium-Ti (10.4 wt %), and low-Ti (1.9 wt %) glasses were selected for focused ion beam cross-section preparation (Fig. 1, D to F, and fig. S2); these cross sections were extracted to simultaneously crosscut the iron-sulfide grains and surrounding glass (Fig. 1, D to F).

Transmission electron microscopy (TEM) data showed that the iron-sulfide grains embedded within Chang'e-5 glass were

[1]Center for Lunar and Planetary Sciences, Institute of Geochemistry, Chinese Academy of Sciences, 550081 Guiyang, China. [2]Planetary Science Institute, State Key Laboratory of Geological Processes and Mineral Resources, School of Earth Sciences, China University of Geosciences, 430074 Wuhan, China. [3]NWU-HKU Joint Center of Earth and Planetary Sciences, Department of Geology, Northwest University, Xi'an 710069, China. [4]State Key Laboratory of Lunar and Planetary Sciences, Macau University of Science and Technology, 999078 Macau, China. [5]Center for Excellence in Comparative Planetology, Chinese Academy of Sciences, 230026 Hefei, China. [6]Planetary Environmental and Astrobiological Research Laboratory, School of Atmospheric Sciences, Sun Yat-Sen University, 519082 Zhuhai, China. [7]Laboratory for Space Environment and Physical Sciences, Harbin Institute of Technology, 150001 Harbin, China. [8]Center for Advanced Mössbauer Spectroscopy, Mössbauer Effect Data Center, Dalian Institute of Chemical Physics, Chinese Academy of Sciences, 116023 Dalian, China.
*Corresponding author. Email: liyang@mail.gyig.ac.cn (Y.L.); he_qi@cug.edu.cn (Q.H.)
†These authors contributed equally to this work.

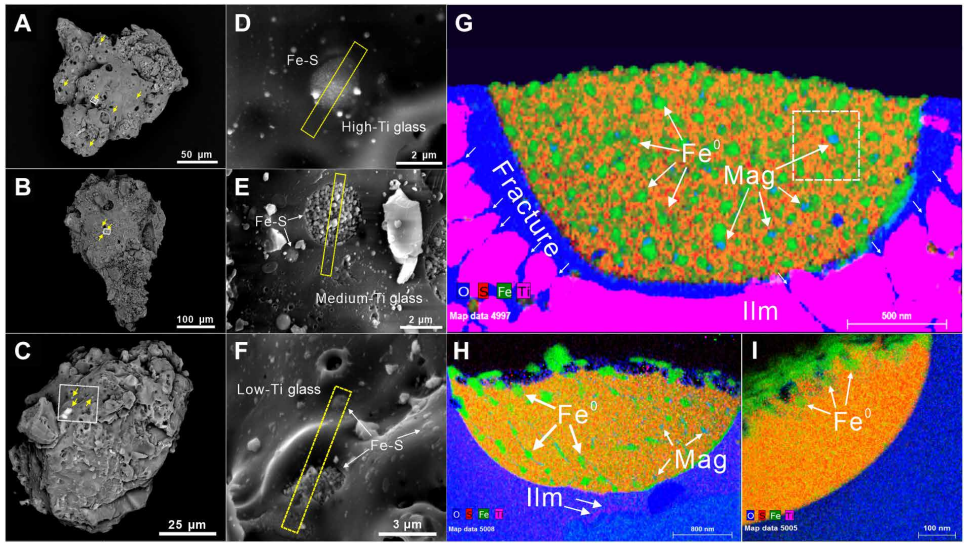

Fig. 1. Droplet-like, rounded iron-sulfide grains embedded within Chang'e-5 glass. (**A** to **F**) Scanning electron microscope (SEM) images of iron-sulfide grains embedded within Chang'e-5 glass containing different amounts of Ti, showing a unique dented microstructural feature on the glass surface. (**G** to **I**) Quantitative energy-dispersive x-ray (EDX) element maps of hemispherical iron-sulfide grains. The iron-sulfide grains in (G) to (I) corresponding to those embedded within high-, medium-, and low-Ti glasses in (D) to (F), respectively. The yellow dashed regions in (D) to (F) are the areas selected for focused ion beam cross-section preparation.

hemispherical, with grain sizes ranging from 300 nm to 2 μm. Quantitative TEM–energy-dispersive x-ray (TEM-EDX) compositional maps revealed markedly variable mineral assemblages and modal abundances within the interior of iron-sulfide grains embedded within glasses of different Ti content (Fig. 1, G to I). In high-Ti glass, abundant submicroscopic magnetite and metallic iron particles were widely distributed within the iron-sulfide grains (Figs. 1G and 2A). With a decrease in Ti content in the glass, the amount of magnetite and metallic iron particles inside the iron-sulfide grains decreased substantially. The interiors of iron-sulfide grains embedded within the medium-Ti glass showed only localized minor coexistence of metallic iron and magnetite. Meanwhile, metallic iron particles and magnetite were absent within the interior of iron-sulfide grains embedded in low-Ti glass (Fig. 1, H and I). These features indicate that the internal mineral assemblage of Chang'e-5 lunar soil sulfides was closely coupled to the composition of the surrounding glass.

Microstructure of iron-sulfide grains

The internal microstructure of iron-sulfide grains embedded within high-Ti glass was more complex compared with those of grains within medium- and low-Ti glasses. The former was tightly enclosed by a radially fractured single ilmenite crystal, and these melt-filled fractures indicate that the impact event caused a localized melting of ilmenite (Fig. 1G and fig. S3A). The presence of such a large ilmenite grain contributes to the high Ti content detected in this glass. The mineral assemblage in the interior of iron-sulfides within high-Ti glass is similar to those of independently occurring Chang'e-5 spherical iron-sulfide grains reported by Guo *et al.* (*17*); both exhibit a large number of submicroscopic pure metallic iron and magnetite particles embedded within a matrix consisting of troilite and pyrrhotite (fig. S3C). Both the structural and compositional data support the occurrence of magnetite within the iron-sulfide grain. TEM-EDX compositional maps and line profiles demonstrated that the magnetite within the iron-sulfide grain was O- and Fe-rich, with a lower sulfur content compared with the iron-sulfide matrix (Figs. 1 and 2 and fig. S6). Electron energy-loss spectroscopy (EELS) Fe L-edge spectra of the magnetite particles within the studied iron-sulfide grain were intermediate between standard Fe^{2+} and Fe^{3+} spectra, indicating the presence of both Fe^{2+} and Fe^{3+} in the magnetite. Quantitative Fe^{3+} EELS data revealed that the magnetite within the studied iron-sulfide grain had an $Fe^{3+}/\sum Fe$ value of 0.63 ± 0.04, which is similar to the theoretical Fe^{3+} content in magnetite (~0.66) (Fig. 2, H and I) (*25*, *26*). In addition, aberration-corrected scanning TEM and high-resolution TEM images of magnetite taken along the [001] zone axis showed lattice fringes with a periodicity of 2.98 Å and an angle of 120°, which can be indexed by the structure of magnetite (Fig. 2B). Collectively, these data confirm that the ubiquitous oxygen-rich phase within iron-sulfide grains embedded within high-Ti glass is magnetite.

In the iron-sulfide grain embedded within medium-Ti glass, a few scattered magnetite particles were observed in the right-hand portion of the grain; a small number of dendritic ilmenite clusters were also present in the lower right portion of the grain, coupled to the location of magnetite (Fig. 1H and fig. S3D). In contrast, metallic iron particles were prevalent both inside and on the surface of this iron-sulfide grain, and these took various shapes (e.g., angular, elongated, and round). These microscopic features imply that the occurrence of magnetite within this iron-sulfide grain is closely related to the ilmenite content of the surrounding glass, while the metallic iron particles are not exclusively related to magnetite formation within the iron-sulfide grain. The metallic iron particles inside and outside the iron-sulfide grain show different modes of occurrence.

No signatures of ilmenite were observed in the low-Ti glass, and the selected area electron diffraction pattern of the iron-sulfide grain embedded within the low-Ti glass showed only the presence of troilite (fig. S3F). There was no magnetite phase inside the iron-sulfide grain, only large metallic iron particles distributed across the surface of the grain (Fig. 1I and fig. S3E).

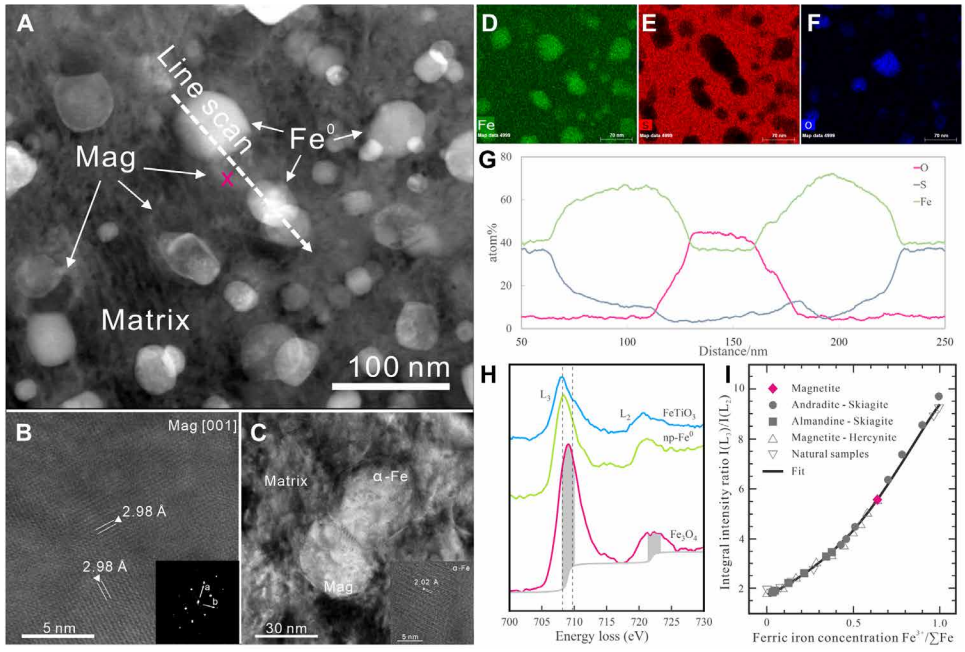

Fig. 2. Internal microstructure of iron-sulfide grains. (**A**) Transmission electron microscope (TEM) bright-field image of an iron-sulfide grain embedded within high-Ti glass, corresponding to the white dashed region in Fig. 1G. (**B**) Aberration-corrected scanning TEM image of magnetite within the same iron-sulfide grain. The fast Fourier transform pattern of the high-resolution TEM image of magnetite is shown in the insert to the bottom right of the figure. (**C**) High-resolution TEM image of submicroscopic pure metallic iron and magnetite particles embedded within a matrix consisting of troilite and pyrrhotite. The aberration-corrected scanning TEM image of the pure metallic iron (α-Fe) particle is shown in the insert to the bottom right of the figure. (**D** to **F**) Quantitative EDX element maps of Fe, S, and O, corresponding to the image in part (A). (**G**) Quantitative TEM–EDX line-profiles obtained from the position indicated by the dotted arrow in (A). (**H** and **I**) Fe $L_{2,3}$ electron energy-loss spectra from a magnetite particle (Fe_3O_4). The measurement point is indicated by the purple cross in (A). A double arctan function was used as a background function to normalize the spectra, and the quantitative results show an approximate Fe^{3+} to ∑Fe ratio of 2:3 in the magnetite particle.

On this basis, we carried out a series of microanalytical work as a statistical result of such magnetite-bearing sulfide grain in the Chang'e 5 lunar soil. We found seven droplet-like iron-sulfide grains with magnetite on the surface of about 200 glassy grains, and the formation of magnetite conforms to the rule we emphasized above in relation to the content of ilmenite or Ti-rich glass (Figs. 1 and 3 and fig. S4).

DISCUSSION

The impact origin on the lunar surface

The distribution and formation mechanism of magnetite in lunar regolith remain unclear (*1*, *12*, *27*, *28*). Our discovery of abundant magnetite particles in droplet-like iron-sulfide grains embedded within high-Ti glass from Chang'e-5 samples suggests a potential prevalence of impact-induced magnetite in high-Ti regions on the Moon (Figs. 1 and 3). Although similar magnetite forms have recently been reported from Chang'e-5 isolated iron-sulfide grains, the absence of surrounding material precluded an accurate assessment of the conditions required for magnetite formation on the lunar surface (*17*).

Here, TEM observations have shown that the studied iron-sulfide grains contain coprecipitated pure metallic iron and magnetite particles, which are in close spatial contact. Such microscopic characteristics of iron-sulfide grains embedded within ilmenite-bearing glass are similar to observations reported in Guo *et al.* (*17*). Therefore, we invoke the same eutectic reaction mechanism ($4FeO = Fe_3O_4 + Fe$) to explain the formation of magnetite and metallic iron particles inside the iron-sulfide grains embedded within Chang'e-5 glass. In addition, previous studies have shown that magnetite can cocrystallize from FeO via a eutectoid reaction (*8*, *17*, *29*, *30*).

The magnetite-bearing iron-sulfide grains were embedded on the surface of impact glass, the radial fracture structure of ilmenite grain, and the boundaries between the iron-sulfide grains and glass substrate coincided perfectly without gap, suggesting that the impact process is the main origin of the formation of such morphologic features (Fig. 1, E and F). Therefore, we propose a specific impact origin for magnetite formation on the lunar surface based on the surrounding chemical environment. The droplet-like, rounded iron-sulfide grains are the reservoirs of submicroscopic magnetite; the potential prevalence of such rounded/dented iron-sulfide microstructure with sharp boundaries on the surface of Chang'e-5 glass is attributed to late cooling shrinkage caused by impact events (Fig. 1, A to F, and fig. S1) (*19*, *21*, *24*). A prerequisite for the production of magnetite inside iron-sulfide droplets is the addition of an oxygen component. Different from the formation of magnetite in iron-sulfides resulting from the addition of dissolved oxygen in large impact gas columns, as suggested by Guo *et al.* (*17*), the occurrence of magnetite in the present study is closely associated with the presence of ilmenite; this implies that the ilmenite component in the glass melts may provide the necessary "oxygen source" for the formation of magnetite inside the Chang'e-5 iron-sulfide grains embedded within glass. The fracture

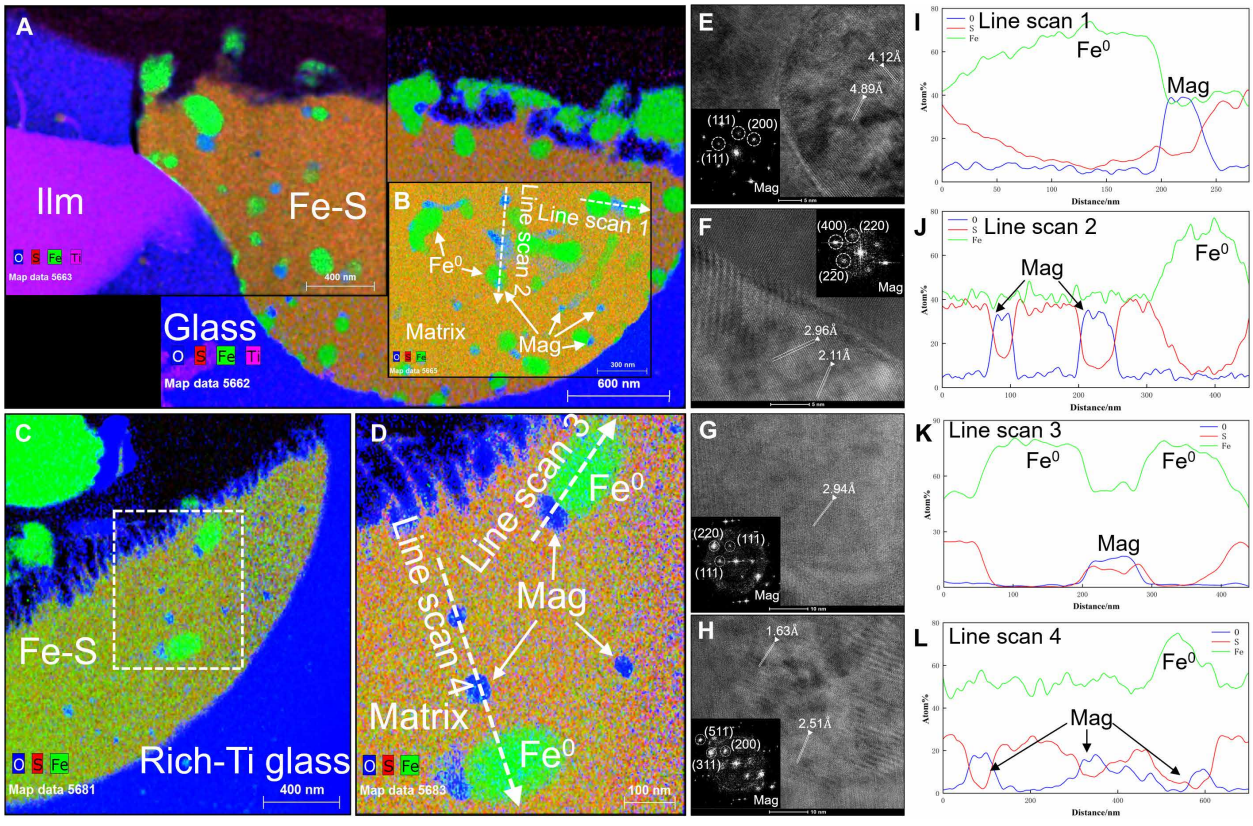

Fig. 3. More examples of hemispherical magnetite-rich iron-sulfide grains embedded within impact glasses. (**A**) Quantitative EDX element maps of hemispherical magnetite-rich iron-sulfide grain. The left side of iron-sulfide grain is in close contact with ilmenite, and there are traces of localized melting and cluster growth at the edge of ilmenite. (**B**) Local quantitative EDX element maps of iron-sulfide grain in (A). (**C**) The EDX element maps of Fe, S, and O in iron-sulfide grain. (**D**) Local quantitative EDX element maps of iron-sulfide grain, corresponding to the white dashed region in (C). (**E** to **H**) High-resolution TEM image of the magnetite particles. The fast Fourier transform pattern is shown in the insert to the corner of the figure. (**I** to **L**) Quantitative TEM–EDX line-profiles obtained from the position indicated by the dotted arrow inside the region in (B) and (D).

and partial melting of the ilmenite grain in the high-Ti glass, and the formation of ilmenite clusters in the medium-Ti glass, suggest that ilmenite melting (~1670°C) occurred and was involved in the reaction during these impact events (Fig. 1, G and H, and fig. S3, A and D). In addition, the formation of magnetite by high-temperature chemical reactions between oxides (e.g., chromite) and sulfides has also been proved in shock-induced melt veins of meteorites (*15*, *31*). Fundamentally, ilmenite is an oxide mineral as chromite. Considering that the oxygen atoms in silicates are bounded by silicon-oxygen tetrahedra, whereas O in ilmenite or chromite is bonded to the metal element mainly in ionic bonds, so that the binding energy of oxygen in silicates is much stronger than the bonding energy in oxides. Therefore, it is highly likely that ilmenite released some of its oxygen into the interior of the sulfide under high-temperature, high-pressure melting conditions induced by the impact on the lunar surface. During the subsequent annealing process, a eutectoid reaction occurs within the interior of O-bearing iron sulfide grains at a temperature below 600°C to form a mineral assemblage with α-Fe, magnetite, and iron-sulfide phases. Numerous metallic iron particles accompanied by abundant pores were observed on the surface of the studied iron-sulfide grains, which are inferred to be the products of later thermal events.

In summary, we found more magnetite-rich iron-sulfide grains to enrich the reliability of our study, and we believe that the impact events between iron-sulfide droplets and ilmenite-bearing glass melts are the key condition for the formation of submicroscopic magnetite on the lunar surface. In the studies on the surface morphology of the various Apollo lunar soil samples, including sampling regions of the mare and highland, the sulfide-droplet-on-glass assemblages of similar composition and structure were also found on the surface of glass bead, agglutinate, and breccia. "Hemispherical mound" was used to describe these sulfides with a unique microstructure, and the formation of them was closely related to impact events (*19*–*24*, *32*–*38*).

The magnetite-rich iron-sulfide grains embedded within high-Ti glasses we found above are just the tip of the iceberg in lunar soil, but this is a positive signal that more magnetite will be found in lunar soil samples with higher glass and TiO_2 content. On the basis of the observed high content of magnetite in high-Ti glass, Ti-rich regions on the Moon may have generally experienced the formation of submicroscopic magnetite under continuous impact modification (Figs. 1, G and H, and 3, A to D). The results of Mössbauer spectroscopy, magnetic separation, and ESR studies during the Apollo era suggest that submicroscopic magnetite particles may be ubiquitous in fine lunar soils, and there is a positive correlation between the

width of ESR "characteristic" resonance lines (i.e., magnetite content) and the TiO_2 content of Apollo lunar soils (*1*, *6*, *10*). In addition, Apollo samples with high Ti content were shown to have a high content of metallic iron or magnetite-like phases, further suggesting a correlation between Ti content and magnetite abundance on the lunar surface (*1*, *5*, *7*, *10*). Therefore, it is highly likely that magnetite is prevalent in Ti-rich regions on the Moon, and the magnetite produced within iron-sulfide grains in ilmenite-bearing glass is likely to represent in situ mineralogical evidence of the magnetite-like phase detected by Mössbauer spectroscopy and ESR in the Apollo era.

The constraints of the impact conditions

The analyses of this unique surface feature in the Apollo samples gave the view that the host surface of glass remains molten or unsolidified liquid phase while capturing the sulfides droplet during the impact event. The microstratigraphy of the sulfides indicates a history of melting, then capture and accumulation of particles (*20*, *21*). The surface morphological observation of magnetite-rich iron-sulfide grains embedded in the impact glass in Chang'e-5 lunar soil shows that the studied iron-sulfide impactor and silicate glass target record no evidence of mechanical fracture or splash of ejecta, and the iron-sulfide impactor is well-preserved with sharp boundaries. All these features indicate that the iron sulfide and silicate glass are not fully solidified at the time of the impact event. The hemispherical iron-sulfide grain with magnetite we studied is a unique category of those sulfide mounds described in Apollo lunar samples. Therefore, the same mechanism of the droplet-on-droplet impact model can be used to understand and constraint the impact scale that drives the formation of magnetite.

To constraint the temperature and pressure conditions of the impact event during the capture of iron-sulfide droplets, we assume that the liquid-phase temperature of Chang'e-5 silicate glass (~1150°C) is the initial target temperature, and the melting point of ilmenite (~1670°C) is the highest postshock temperature. The functional relationship between postshock temperature and shock pressure for minerals shocked at room temperature shows that a temperature increase of about 520°C corresponds to an impact pressure of approximately 42 GPa (fig. S5A) (*39*–*41*). According to the Hugoniot equations, a particle velocity of approximately 1.65 km/s was calculated to achieve an ideal pressure of 42 GPa (fig. S5B) (*40*, *42*, *43*). Such a low velocity falls within the range of secondary impact velocities on the lunar surface, which likely result from the mutual collision of ejecta material arising from large impact events (*18*). After the contact and compression stage of shocking, the peak pressure dissipates rapidly and is released to ~2 to 5 GPa inside ilmenite and disappears in the melt. Therefore, the high-pressure environment promotes the dissolution of FeO as an oxygen source in iron-sulfide droplets, forming magnetite via a eutectoid reaction.

Previous studies have confirmed that the magnetic anomaly distribution in the lunar crust may be related to ejecta of large impacts; the potentially ubiquitous production of ferromagnetic minerals reported in this study provides further support for an impact-induced mechanism for lunar surface magnetic anomalies (*17*, *44*). The sulfides in the liquid outer core and ilmenite carried by the early lunar mantle overturning events came into contact with each other in the high-pressure environment (~4.75 GPa) of the lunar core-mantle boundary may have resulted in the presence of dissolved oxygen in the sulfide and the formation of magnetite in the deep Moon (*45*–*50*).

MATERIALS AND METHODS

This study used the Chang'e-5 lunar soil samples CE5C0200, CE5Z1002YJ, CE5Z0806YJ, CE5Z0403YJFM002H, and CE5Z0204YJ. Each lunar soil sample was affixed to conductive carbon adhesive tape under an optical microscope and observed under an SEM.

A large number of iron-sulfide grains were observed in lunar fine-grained material using back-scattered electron imaging, and the composition and morphology of these grains were preliminarily determined using EDX analysis within a field-emission SEM (FEI Scios) at the Institute of Geochemistry, Chinese Academy of Sciences (CAS), Guiyang. Nanophases within the samples were characterized using field-emission scanning TEM (FEI Talos F200X) at the Suzhou Institute of Nano-tech and Nano-bionics, CAS. Accurate quantification of compositional data was performed using an interactive TEM-EDX method. Nanoscale crystal structures were analyzed and identified using high-resolution TEM images and selected-area electron diffraction patterns.

To measure the oxidation state of Fe in nanocrystals within iron-sulfide grains, EELS spectra were acquired using a Hitachi HF5000 aberration-corrected scanning TEM (Hitachi) equipped with a Gatan GIF Quantum ER System Model 965 parallel EELS spectrometer at the Shanghai Institute of Ceramics, CAS. The EELS spectra were collected in DualEELS mode with a probe current of 100 pA. Quantitative analysis of $Fe^{3+}/\sum Fe$ within Fe-oxide particles was performed via systematic empirical fitting of the integral part of the Gaussian curve through the method of the modified integral intensity ratio of the Fe $L_{2,3}$ "white line." We used the position of the white line (sharp maxima) of the Fe^0 of the metallic iron and Fe^{2+} of ilmenite in the samples (708.2 eV) as an internal calibration of the samples. The L_3 and L_2 edges of both Fe^{2+} and Fe^{3+} showed substantial splitting, with the maximum distance (spin-orbit splitting) of the white line being 12.8 ± 0.1 eV and 13.2 ± 0.1 eV, respectively (*25*, *51*). In general, Fe^{2+} and Fe^{3+} L_3 are separated by approximately 1.5 eV at the beginning of the white line (*52*), which is calibrated to be 709.7 eV for ferric Fe L_3 of these particles.

Detailed information regarding the magnetite chemical composition quantitation and impact history inversion is given in the Supplementary Materials.

Supplementary Materials

This PDF file includes:

Supplementary Text
Figs. S1 to S6
References

REFERENCES AND NOTES

1. D. L. Griscom, E. J. Friebele, C. L. Marquardt, Evidence for a ubiquitous, sub-microscopic "magnetite-like" constituent in the lunar soils. *Proc. Lunar Sci. Conf.* **4**, 2709–2727 (1973).
2. M. Wadhwa, Redox conditions on small bodies, the Moon and Mars. *Rev. Mineral. Geochem.* **68**, 493–510 (2008).
3. K. D. Burgess, R. M. Stroud, Coordinated nanoscale compositional and oxidation state measurements of lunar space-weathered material. *J. Geophys. Res. Planets* **123**, 2022–2037 (2018).
4. S. Li, P. G. Lucey, A. A. Fraeman, A. R. Poppe, V. Z. Sun, D. M. Hurley, P. H. Schultz, Widespread hematite at high latitudes of the Moon. *Sci. Adv.* **6**, eaba1940 (2020).
5. P. Gay, G. M. Bancroft, M. G. Bown, Diffraction and Mössbauer studies of minerals from lunar soils and rocks. *Science* **167**, 626–628 (1970).
6. D. L. Griscom, C. L. Marquardt, Evidence of lunar surface oxidation processes: Spin resonance spectra of lunar materials and simulated lunar materials. *Proc. Lunar Sci. Conf.* **3**, 2397 (1972).

7. R. Housley, R. Grant, M. Abdel-Gawad, Study of excess Fe metal in the lunar fines by magnetic separation, Mössbauer spectroscopy, and microscopic examination. *Proc. Lunar Sci. Conf.* **3**, 1065 (1972).
8. R. J. Williams, E. K. Gibson, The origin and stability of lunar goethite, hematite and magnetite. *Earth Planet. Sci. Lett.* **17**, 84–88 (1972).
9. D. W. Forester, C. L. Marquardt, D. L. Griscom, Mössbauer search for ferric oxide phases in lunar materials and simulated lunar materials. *Lunar Planet. Sci. Conf. Proc.* **4**, 257 (1973).
10. D. L. Griscom, C. L. Marquardt, The origin and significance of the "characteristic" ferromagnetic resonance of lunar soils: Two views. *Lunar Planet. Sci. Conf. Proc.* **4**, 320–322 (1973).
11. C. K. Shearer, Z. D. Sharp, P. V. Burger, F. M. Mccubbin, P. P. Provencio, A. J. Brearley, A. Steele, Chlorine distribution and its isotopic composition in "rusty rock" 66095. Implications for volatile element enrichments of "rusty rock" and lunar soils, origin of "rusty" alteration, and volatile element behavior on the Moon. *Geoch. Cosm. Act.* **139**, 411–433 (2014).
12. K. H. Joy, C. Visscher, M. E. Zolensky, T. Mikouchi, K. Hagiya, K. Ohsumi, D. A. Kring, Identification of magnetite in lunar regolith breccia 60016: Evidence for oxidized conditions at the lunar surface. *Meteorit. Planet. Sci.* **50**, 1157–1572 (2015).
13. P. J. Wasilewski, Shock remagnetization associated with meteorite impact at planetary surfaces. *Moon* **6**, 264–291 (1973).
14. H. Y. Mcsween, A new type of chondritic meteorite found in lunar soil. *Earth Planet. Sci. Lett.* **31**, 193–199 (1976).
15. M. Chen, X. Xie, D. Wang, S. Wang, Metal-troilite-magnetite assemblage in shock veins of Sixiangkou meteorite. *Geochim. Cosmochim. Acta* **66**, 3143–3149 (2002).
16. G. Heiken, D. Vaniman, B. M. French, *Lunar Sourcebook: A User's Guide to the Moon* (Cambridge Univ. Press, Cambridge, 1991).
17. Z. Guo, C. Li, Y. Li, Y. Wen, Y. Wu, B. Jia, K. Tai, X. Zeng, X. Li, J. Liu, Z. Ouyang, Sub-microscopic magnetite and metallic iron particles formed by eutectic reaction in Chang'E-5 lunar soil. *Nat. Commun.* **13**, 7177 (2022).
18. C. Li, Z. Guo, Y. Li, K. Tai, K. Wei, X. Li, J. Liu, W. Ma, Impact-driven disproportionation origin of nanophase iron particles in Chang'e-5 lunar soil sample. *Nat. Astron.* **6**, 1156–1162 (2022).
19. P. Yan, Z. Xiao, Y. Wu, W. Yang, J. H. Li, L. X. Gu, S. Liao, Z. Yin, H. Wang, H. C. Tian, C. Zhang, S. Wu, H. X. Ma, X. Tang, S. T. Wu, H. Hui, Y. Xu, W. Hsu, Q. L. Li, F. Luo, Y. Liu, X. H. Li, Intricate regolith reworking processes revealed by microstructures on lunar impact glasses. *J. Geophys. Res. Planets* **127**, e2022JE007260 (2022).
20. J. L. Carter, I. D. Macgregor, Mineralogy, petrology, and surface features of some Apollo 11 samples. *Lunar Planet. Sci. Conf. Proc.* **1**, 247–265 (1970).
21. D. S. Mckay, W. R. Greenwood, D. A. Morrison, Origin of small lunar particles and breccia from the Apollo 11 site. *Geochim. Cosmochim. Acta* **1**, 673 (1970).
22. J. L. Carter, Chemistry and surface morphology of fragments from Apollo 12 soil. *Lunar Planet. Sci. Conf. Proc.* **2**, 873 (1971).
23. J. L. Carter, D. S. Mckay, Metallic mounds produced by reduction of material of simulated lunar composition and implications on the origin of metallic mounds on lunar glasses. *Lunar Planet. Sci. Conf. Proc.* **3**, 953 (1972).
24. J. L. Carter, Chemistry and surface morphology of soil particles from Luna 20 LRL sample 22003. *Geochim. Cosmochim. Acta* **37**, 795–803 (1973).
25. P. A. Van Aken, B. Liebscher, V. J. Styrsa, Quantitative determination of iron oxidation states in minerals using Fe $L_{2,3}$-edge electron energy-loss near-edge structure spectroscopy. *Phys. Chem. Miner.* **25**, 323–327 (1998).
26. P. A. Van Aken, B. Liebscher, Quantification of ferrous/ferric ratios in minerals: New evaluation schemes of Fe L 23 electron energy-loss near-edge spectra. *Phys. Chem. Miner.* **29**, 188–200 (2002).
27. J. Jedwab, A. Herbosch, R. Wollast, G. Naessens, N. Van Geen-Peers, Search for magnetite in lunar rocks and fines. *Science* **167**, 618–619 (1970).
28. D. W. Collinson, A. Stephenson, S. K. Runcorn, Magnetic properties of Apollo 15 and 16 rocks. *Lunar Planet. Sci. Conf. Proc.* **4**, 2963 (1973).
29. O. I. Yakovlev, Y. P. Dikov, M. V. Gerasimov, Effect of the disproportionation reaction of ferrous iron in impact-evaporation processes. *Geochem. Int.* **47**, 134–142 (2009).
30. Y. Shizukawa, S. Hayashi, S. Yoneda, Y. Kondo, H. Tanei, S. Ukai, Mechanism of magnetite seam formation and its role for FeO scale transformation. *Oxid. Met.* **86**, 315–326 (2016).
31. P. Gillet, M. Chen, L. Dubrovinsky, A. E. Goresy, Natural $NaAlSi_3O_8$-hollandite in the shocked Sixiangkou meteorite. *Science* **287**, 1633–1636 (2000).
32. J. B. Hartung, F. Hörz, D. S. Mckay, F. L. Baiamonte, Surface features on glass spherules from the Luna 16 sample. *Moon* **5**, 436–446 (1972).
33. J. L. Carter, Morphology and chemistry of probable VLS (vapor-liquid-solid)-type of whisker structures and other features on the surface of breccia 15015,36. *Lunar Planet. Sci. Conf. Proc.* **4**, 413 (1973).
34. J. L. Carter, H. C. J. M. Taylor, E. Padovani, J. L. Carter, H. C. J. Taylor, E. Padovani, Morphology and chemistry of particles from Apollo 17 soils 74220, 74241 and 75081. *EOS Trans. AGU* **54**, 580–622 (1973).
35. D. S. Mckay, U. S. Clanton, G. Ladle, Scanning electron microscope study of Apollo 15 green glass. *Lunar Planet. Sci. Conf. Proc.* **4**, 225 (1973).
36. G. H. Heiken, D. S. Mckay, R. W. Brown, Lunar deposits of possible pyroclastic origin. *Geochim. Cosmochim. Acta* **38**, 1703–1704 (1974).
37. J. Butler, C. Meyer, Sulfur prevails in coatings on glass droplets—Apollo 15 green and brown glasses and Apollo 17 orange and black/devitrified/glasses. *Lunar Planet. Sci. Conf. Proc.* **7**, 1561–1581 (1976).
38. C. D. Stone, L. A. Taylor, D. S. Mckay, R. V. Morris, Ferromagnetic resonance intensity: A rapid method for determining lunar glass bead origin. *J. Geophys. Res.* **87**, A182–A196 (1982).
39. S. A. Raikes, T. J. Ahrens, Post-shock temperatures in minerals. *Geophys. J. Int.* **58**, 717–747 (1979).
40. D. Stöffler, K. Keil, E. R. D. Scott, Shock metamorphism of ordinary chondrites. *Geochim. Cosmochim. Acta* **55**, 3845–3867 (1991).
41. T. Long, Y. Qian, M. D. Norman, K. Miljkovic, C. Crow, J. W. Head, X. Che, R. Tartèse, N. Zellner, X. Yu, S. Xie, M. Whitehouse, K. H. Joy, C. R. Neal, J. F. Snape, G. Zhou, S. Liu, C. Yang, Z. Yang, C. Wang, L. Xiao, D. Liu, A. Nemchin, Constraining the formation and transport of lunar impact glasses using the ages and chemical compositions of Chang'e-5 glass beads. *Sci. Adv.* **8**, eabq2542 (2022).
42. D. Stoffler, Density of minerals and rocks under shock compression, in Landolt-Börnstein–Numerical Data and Functional Relationships in Science and Technology. New Series, Group V: Geophysics and Space Research (Springer-Verlag, 1982), vol. 1, Sub-vol. A, pp. 120–183.
43. T. G. Sharp, P. S. Decarli, Shock Effects in Meteorites, in *Meteorites and the Early Solar System II*, D. S. Lauretta and H. Y. McSween Jr. Eds. (University of Arizona Press, Tucson, 2006).
44. M. A. Wieczorek, B. P. Weiss, S. T. Stewart, An impactor origin for lunar magnetic anomalies. *Science* **335**, 1212–1215 (2012).
45. B. Mason, Composition of the Earth. *Nature* **211**, 616–618 (1966).
46. V. Rama Murthy, H. T. Hall, The chemical composition of the Earth's core: Possibility of sulphur in the core. *Phys. Earth Planet. Inter.* **2**, 276–282 (1970).
47. V. Rama Murthy, H. T. Hall, The origin and chemical composition of the earth's core. *Phys. Earth Planet. Inter.* **6**, 123–130 (1972).
48. P. S. Balog, R. A. Secco, D. C. Rubie, D. J. Frost, Equation of state of liquid Fe-10 wt % S: Implications for the metallic cores of planetary bodies. *J. Geophys. Res. Solid Earth* **108**, 2001JB001646 (2003).
49. R. F. Garcia, J. Gagnepain-Beyneix, S. Chevrot, P. Lognonné, Very preliminary reference Moon model. *Phys. Earth Planet. Inter.* **188**, 96–113 (2011).
50. R. C. Weber, P.-Y. Lin, E. J. Garnero, Q. Williams, P. Lognonné, Seismic detection of the lunar core. *Science* **331**, 309–312 (2011).
51. C. Colliex, T. Manoubi, C. Ortiz, Electron-energy-loss-spectroscopy near-edge fine structures in the iron-oxygen system. *Phys. Rev. B* **44**, 11402–11411 (1991).
52. L. A. J. Garvie, P. R. Buseck, Ratios of ferrous to ferric iron from nanometre-sized areas in minerals. *Nature* **396**, 667–670 (1998).
53. T. J. Ahrens, Equations of state of iron sulfide and constraints on the sulfur content of the Earth. *J. Geophys. Res. Solid Earth* **84**, 985–998 (1979).
54. J. M. Brown, T. J. Ahrens, D. L. Shampine, Hugoniot data for pyrrhotite and the Earth's core. *J. Geophys. Res. Solid Earth* **89**, 6041–6048 (1984).
55. H. J. Melosh, *Impact Cratering: A Geologic Process* (Oxford Univ. Press, Oxford, 1989).
56. G. S. Collins, H. J. Melosh, G. R. Osinski, The impact-cratering process. *Elements* **8**, 25–30 (2012).
57. H. J. Melosh, The Contact and Compression Stage of Impact Cratering, in *Impact Cratering* G. R. Osinski and E. Pierazzo Eds. (John Wiley & Sons, Hoboken, 2012).

Acknowledgments: We thank all the staff of the Chang'e lunar exploration project for the hard work and CNSA for providing access to the Lunar samples CE5C0200, CE5Z1002YJ, CE5Z0806YJ, CE5Z0403YJFM002H, and CE5Z0204YJ. **Funding:** This work was financially supported by Strategic Priority Research Program of the Chinese Academy of Sciences grant XDB 41000000 (Y.L.); National Natural Science Foundation of China (42303039, 42273042, and 41931077); "From 0 to 1" Original Exploration Cultivation Project, Institute of Geochemistry, Chinese Academy of Sciences (DHSZZ2023-3); the Youth Innovation Promotion Association, Chinese Academy of Sciences (2020395); the China Postdoctoral Science Foundation (2023T160006); and the Pre-Research Project on Civil Aerospace Technologies (D020205).
Author contributions: Z.C. and Z.G. contributed equally to the conception, methodology, investigation, and paper writing of this study. C.L., S.Z., and Y.W. contributed to the methodology and investigation. Y.L. and Q.H. were responsible for the conception, investigation, supervision, paper revision, and funding acquisition. Z.X., X.L., L.X., L.L., J.W., and J.L. contributed to the manuscript discussions. **Competing interests:** The authors declare that they have no competing interests. **Data and materials availability:** All data needed to evaluate the conclusions in the paper are present in the paper, the Supplementary Materials, and online at https://data.mendeley.com/datasets/3wwkcgn42r/2.

Submitted 29 November 2023
Accepted 16 August 2024
Published 20 September 2024
10.1126/sciadv.adn2301